Chemical Engineering Journal 548 (2026) 181577

Contents lists available at ScienceDirect

Chemical Engineering Journal

journal homepage: www.elsevier.com/locate/cej

Bio-inspired hierarchical flexible fabric glove enables low-cost full-palm tactile sensing

Yunsheng Ma, Xinran Li, Jiayi Wen, Jiaxin Huang, Hanyu Liu, Keqiang Ren, Tao Jian, Zhihua Wang, Zhigong Song *

Jiangsu Provincial Key Laboratory of Food Advanced Manufacturing Equipment Technology, School of Mechanical Engineering, Jiangnan University, Wuxi, 214122, China

A R T I C L E I N F O

Keywords:
Wearable tactile sensing
Flexible fabric tactile glove
Full-palm tactile array
Matrix scanning
Low-cost tactile interface
Human–machine interaction

A B S T R A C T

Wearable tactile sensing systems have long faced a trilemma in which wide-area sensing, flexible conformability, and low-cost integration are difficult to achieve simultaneously. Inspired by the functional hierarchy of human skin, this work presents a bio-inspired flexible fabric tactile glove with a hierarchical sensing architecture that integrates pressure sensing, node addressing, and signal transmission into the textile body. An orthogonal conductive-yarn array combined with time-division-multiplexed matrix scanning forms a full-palm tactile array containing 225 addressable nodes. Under normal matrix-scanning operation, the glove exhibits system-level apparent response and recovery times of approximately 90 ms and 80 ms, respectively. A representative sensing node shows an experimentally verified minimum detectable pressure of 0.4 kPa and a monotonic pressure response over 0–400 kPa. After 6000 repeated loading cycles, the response-amplitude retention is 99.4%. The material cost of one tactile glove together with its basic readout circuitry is approximately US$5, while the fabric structure retains its flexibility, conformability, and breathability. Experiments involving dexterous-hand teleoperation, shared tactile feedback, and exoskeleton-assistance triggering further demonstrate the feasibility of using the glove as a low-cost tactile interface for human–machine interaction.

1. Introduction

The hand is the primary human interface for grasping, pressing, and fine manipulation [1–3]. Its motor control depends not only on visual guidance, but also on real-time tactile perception of contact location, loading state, and their dynamic variations [4–6]. With the development of intelligent interaction technologies, accurate acquisition of hand tactile information has become essential for improving operational stability, interaction naturalness, and task reliability [7–11]. Particularly in contact-rich scenarios such as robotic dexterous manipulation [12–14], skill transfer [15,16], and remote interaction [17,18], vision can describe object geometry and spatial position but cannot directly reflect contact states or force variations, which may compromise interaction stability [19–21]. Tactile information arises from direct hand–object contact and can reflect the mechanical state of an interaction in real time [22–24], thereby supporting motion adjustment and task execution [25,26]. Tactile gloves capable of synchronously acquiring contact information from the five fingers and palm during natural hand motion are therefore becoming important platforms for hand tactile-data acquisition and human–machine interaction.

To acquire hand tactile information, several representative tactile glove systems have been developed. OSMO [27] arranges 12 PCB tactile units at the fingertips and palm to collect contact information during natural operation. However, the small number and discrete distribution of sensing nodes make it difficult to obtain continuous, fine-grained full-palm pressure information, and the PCB modules remain add-on components rather than being integrated with the glove body. Ruppel et al. [28] designed an elastic glove containing 102 capacitive tactile units, improving sensing coverage and deformation adaptability over the fingers and palm. Nevertheless, its spatial resolution remains limited for continuous high-density full-palm sensing, and the breathability and long-term wearing comfort of the continuous silicone-rubber membrane are inferior to those of textile materials. STAG [29] constructs a full-palm tactile array with 548 sensing units by attaching a piezoresistive sensing layer to a knitted glove. Although this substantially expands the sensing area, the external array layer can reduce the original flexibility

* Corresponding author.
E-mail address: song_jnu@jiangnan.edu.cn (Z. Song).

https://doi.org/10.1016/j.cej.2026.181577
Received 1 June 2026; Received in revised form 7 August 2026; Accepted 3 September 2026
Available online 4 September 2026

and breathability of the glove, while the complex wiring increases system integration complexity. OPENTOUCH [30] uses flexible printed circuit boards to construct tactile arrays, reducing the complexity of manual wiring and sensor assembly and improving fabrication consistency. However, it still relies on an add-on sensing structure composed of FPCs and piezoresistive films, with limitations in breathability, compliant deformation, and long-term wearability. Luo et al. [31] further integrated conductive yarns and piezoresistive materials into a textile glove through digital embroidery, reflecting the transition of tactile gloves from add-on sensors toward fabric-based sensing structures. This approach offers good flexibility, breathability, and low-cost fabrication, but contains only 23 tactile units and therefore remains insufficient for continuously reconstructing the spatial pressure distribution over the five fingers and palm.

Overall, large-area flexible pressure-sensing matrices can bend but are often unable to conform sufficiently to the complex curved geometry of the hand [32–34]. Bio-inspired electronic skins provide good flexible conformability, yet generally rely on complex structures and fabrication processes that hinder low-cost deployment [35–38]. Flexible textile sensors combine softness with cost advantages, but their sensing-node count and coverage remain limited [39,40]. Existing technologies therefore face a mutually constraining trilemma among wide-area sensing, flexible conformability, and low-cost integration [17,21,41]. Achieving stable acquisition and matrix representation of multipoint pressure information over the full palm, together with low-cost fabrication, while retaining a lightweight, soft, and comfortable glove remains a key challenge for tactile gloves for data acquisition.

As shown in Fig. 1, to address these issues, inspired by the hierarchical tactile sensing mechanism of human skin, this work proposes a bio-inspired hierarchical piezoresistive full-palm tactile fabric glove that serves as a tactile interaction interface to mitigate the trilemma among wide-area sensing, flexible conformability, and low-cost integration. The glove integrates a flexible fabric substrate, conductive-yarn networks, a piezoresistive sensing material, and an insulating layer into a functional hierarchy inspired by the coordinated organization of contact, sensing, and information transmission in human skin. Unlike conventional approaches that attach discrete sensors, circuits, or flexible arrays to the glove surface [27,29], the conductive yarns and piezoresistive material are directly integrated into the multilayer fabric structure on the palmar side, allowing the glove body to provide structural support during wear, pressure transmission, electromechanical conversion, and signal transmission. The glove is mainly fabricated from polyester fabric, stainless-steel conductive yarns, and carbon-containing piezoresistive fabric using conventional sewing and interlayer assembly. The material cost of one glove together with its basic readout circuitry is approximately US$5 (Supplementary **Table S1**). An orthogonal conductive-yarn array and time-division-multiplexed matrix scanning enable multipoint pressure acquisition and matrix representation over the five fingers and palm using a limited number of leads, reducing the dependence of high-density tactile arrays on complex wiring and independent hardware channels. The resulting glove combines fabric softness, conformability, and breathability with low-cost, scalable full-palm tactile acquisition. Based on this design, the following sections analyze the glove structure and sensing mechanism, characterize its sensing performance, and validate its use in dexterous-hand teleoperation, shared tactile feedback, and exoskeleton-assistance triggering for representative motion-mapping, tactile-transmission, and task-triggering applications.

2. Structural design and sensing mechanism of the bio-inspired hierarchical flexible fabric glove

Human skin can reliably perceive external stimuli during complex contact processes such as grasping, pressing, and sliding. This capability does not arise from isolated sensing units, but from the coordinated functions of multilayer tissues that collectively accomplish tactile-information acquisition, conversion, and transmission. The epidermis, which is directly exposed to the external environment, forms a compliant contact and mechanically protective interface. The dermis and subcutaneous tissues are soft and deformable, allowing local contact loads to be transmitted and redistributed internally. Tactile receptors embedded within the skin respond to mechanical stimuli and transmit information to the central nervous system through neural pathways. Tactile perception in human skin is therefore not a simple pressure–response process, but a hierarchically coordinated mechanism involving a contact interface, a mechanical transmission medium,

Fig. 1. Design concept and potential application scenarios of the bio-inspired hierarchical flexible fabric glove. **a** Robot skill learning and transfer based on tactile demonstrations; **b** shared tactile feedback through cross-end conversion of full-palm pressure signals; **c** full-palm tactile input for robotic dexterous manipulation; **d** hand-contact intention sensing for exoskeleton assistance control.

sensory conversion units, and signal-transmission pathways. Inspired by this mechanism, tactile sensing functionality is embedded into the fabric structure on the palmar side of the glove, enabling the glove body to provide structural support during wear, pressure transmission, electromechanical conversion, and signal transmission within an integrated functional hierarchy.

As shown in Fig. 2a, the hierarchical tactile sensing mechanism of human skin provides functional inspiration for the organization of the glove. The outer flexible fabric layer forms the direct contact interface and establishes compliant contact with objects while transmitting external pressure. The intermediate piezoresistive layer converts pressure stimuli into electrical responses. The upper and lower conductive-yarn networks perform node addressing and signal transmission, whereas the insulating layer restricts conduction in non-target regions and reduces array interference. The coordinated functions of contact, sensing, and information transmission in human skin are thereby engineered into a “fabric contact–piezoresistive conversion–array addressing–signal readout” process in the glove.

The pressure-sensing region covers the five fingers and palm and is sewn to the remaining polyester fabric substrate to form a complete glove. To accommodate natural hand bending while providing full-palm coverage and array-based sensing, the palmar region is constructed as a flexible hierarchical composite. As shown in Fig. 2b, from the near-palm side to the far-palm side, the structure sequentially comprises a near-palm conductive layer, an insulating layer, a piezoresistive layer, and a far-palm conductive layer. Rather than being merely stacked, these layers form a functionally complementary tactile sensing structure: the conductive layers provide signal input, node addressing, and output; the piezoresistive layer converts pressure into resistance changes; the insulating layer defines the effective sensing regions; and the fabric substrate enables the overall structure to bend naturally and conform to the hand surface.

After array alignment, the conductive, insulating, and piezoresistive layers are sewn together only along the finger contours and outer palm boundary, with local reinforcement stitches added near the finger roots, palm edge, and lead outlet where relative displacement is more likely to occur. No continuous bonding is applied within the functional areas, and the stitches are positioned mainly outside the effective tactile nodes to minimize local compression of the piezoresistive layer. This edge-constrained fixation prevents gross interlayer misalignment while permitting limited relative sliding and local separation during hand bending. Consequently, in-plane bending strain is not fully transferred to the piezoresistive layer, and local interlayer gaps partly buffer bending-induced compression, providing a degree of passive mechanical

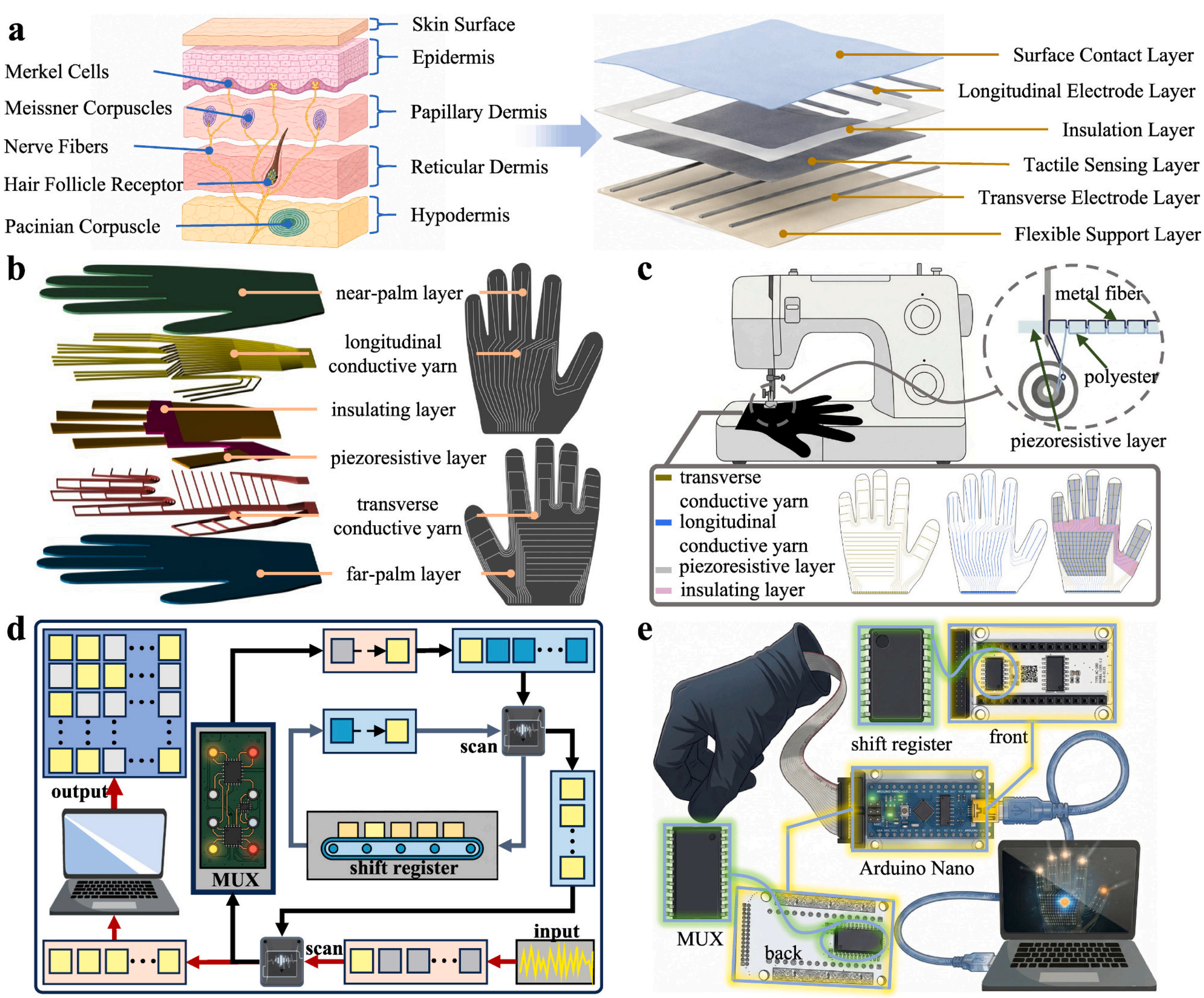

Fig. 2. Functional hierarchical structure and tactile sensing mechanism of the Bio-inspired Hierarchical Flexible Fabric Glove. a Design inspiration from the coordinated hierarchical tactile sensing of human skin; **b** exploded view of the hierarchical fabric structure of the tactile glove; **c** conductive-yarn stitching and routing process and its spatial distribution in the glove; **d** time-division-multiplexed tactile matrix scanning; e overall connection of the tactile glove, external control circuit, and host-computer visualization system.

decoupling.

The near-palm conductive layer uses flexible fabric as the substrate. Ordinary yarn is used as the bobbin thread and stainless-steel conductive yarn as the needle thread; continuous and orderly longitudinal conductive paths can therefore be formed along the finger direction using the flat-stitching process of a conventional household sewing machine without special attachments (Supplementary **Fig. S1**). In the stitch structure, the stainless-steel conductive yarn is continuously constrained by periodically spaced bobbin-thread loops. If local metal filaments become loose or break during prolonged use, adjacent stitches can limit their range of motion to some extent, reducing the likelihood that they extend toward and bridge neighboring conductive paths. This layer participates in the spatial encoding and signal acquisition of tactile nodes and transmits local electrical responses, thereby providing the structural basis for orderly readout of full-palm tactile information. Considering finger width and contact-area distribution, three longitudinal sensing paths are arranged on each finger to cover the center and both sides of the finger pad. A total of 15 parallel longitudinal conductive traces are formed over the five fingers and extended into the palm, providing continuous tactile coverage of the finger and palm regions.

The piezoresistive layer is located between the two conductive layers and serves as the core electromechanical conversion layer of the glove. It is composed of carbon-containing piezoresistive fabric whose resistance decreases nonlinearly with increasing applied mass, exhibiting a pronounced negative piezoresistive response (Supplementary **Figs. S2** and **S3**). When the hand contacts an object, pressure is transmitted through the outer fabric layer to the piezoresistive layer, changing the local contact state and conductive network. The resulting resistance response is read at the intersections of the upper and lower stainless-steel conductive yarns. The stainless-steel conductive yarn also exhibits relatively consistent resistance per unit length (Supplementary **Fig. S4**), supporting stable array signal transmission and node addressing. Functionally, this process corresponds to mechanical stimulation acting on tactile receptors in human skin and producing neural signals; in the proposed fabric glove, however, contact pressure is converted into a measurable electrical signal.

The far-palm conductive layer adopts the same stitching process as the near-palm conductive layer, but the conductive yarns are arranged transversely across the palm and form an orthogonal array with the longitudinal traces. Each intersection of the longitudinal and transverse conductive traces forms an addressable tactile node through the intermediate piezoresistive layer, allowing a full-palm tactile array to be constructed without placing a separate sensor at every location. This arrangement expands sensing coverage while reducing wiring complexity. As shown in Fig. 2c, four cross-finger transverse paths are arranged in the finger region of the far-palm conductive layer. One path crosses the fingertip region of each finger to acquire fingertip pressure, while the other three are distributed near the finger joints to collect contact- and deformation-related responses. Eleven additional parallel transverse traces are arranged in the palm. Together with the 15 longitudinal paths of the near-palm conductive layer, they form a 15 × 15 tactile array containing 225 addressable nodes for matrix-based representation of the pressure distribution over the five fingers and palm.

Integrating multiple functions on a limited hardware platform is an effective means of reducing system size and simplifying hardware [42]. A tactile-network control system was therefore developed for efficient readout of full-palm tactile information. Providing an independent signal channel for each of the 225 nodes would substantially increase wiring complexity, hardware cost, and the connection burden at the wrist, while reducing glove flexibility and wearing comfort. As shown in Fig. 2d, the system combines shift registers and a multiplexer to sequentially select row and column channels according to a predefined timing sequence and complete tactile-matrix scanning through time-division multiplexing. Multiple tactile nodes can thus share a limited number of acquisition and transmission channels, enabling continuous readout of full-palm multipoint pressure signals with reduced hardware complexity. The tactile glove itself, including the glove substrate, multilayer sensing structure, conductive yarns, and wrist connection leads, weighs approximately 60 g; the external control electronics, computer, and power supply are not included.

Based on the above structure, the tactile sensing process can be summarized as four consecutive stages: contact, conversion, addressing, and readout. When the hand contacts an object, external pressure first acts on the flexible fabric surface and is transmitted through the contact layer to the internal piezoresistive layer. Local compression changes the resistance of the piezoresistive layer, completing electromechanical conversion. The upper and lower orthogonal conductive-yarn layers then spatially address the local response so that the pressure information corresponds to a specific row–column intersection. Finally, the control system sequentially reads the response of each node according to the predefined timing sequence and reconstructs a full-palm tactile matrix.

As shown in Fig. 2e, the tactile glove is electrically connected to external connection leads by soldering (Supplementary **Fig. S5**). Before soldering, a flux suitable for stainless steel is applied to the ends of the conductive yarns, followed by pre-tinning. The flux improves solder wettability and adhesion and can also carry away part of the heat during volatilization, thereby reducing local heat accumulation to some extent. Pre-tinning further gathers and fixes loose metallic filaments at the yarn ends, reducing the risk of bridging and short circuits between adjacent conductive paths. Short-duration, localized heating is used during soldering to minimize thermal exposure of the textile substrate. In addition, the connection region is located at the wrist, away from the main bending and tactile-sensing regions of the fingers and palm, which helps reduce direct mechanical loading on the solder joints and minimizes the influence of local thermal effects and stiffening on the overall flexibility and tactile sensing performance of the glove. The connection leads are then interfaced with the PCB control board, which communicates with the host computer through an Arduino module. The host computer converts the contact information distributed over the five fingers and palm into intuitive tactile images (Supplementary **Figs. S6** and **S7**), supporting gesture analysis, grasp-state analysis, robot teleoperation, and tactile feedback.

Taken together, the flexible fabric substrate, orthogonal conductive yarns, piezoresistive sensing layer, and insulating auxiliary layer cooperatively integrate tactile sensing into the glove body. The structure uses low-cost, readily available commercial textile materials and can be fabricated by conventional sewing and interlayer assembly without complex equipment or a cleanroom environment. Meanwhile, the 15 × 15 orthogonal array and time-division-multiplexed scanning reduce the dependence of high-density full-palm sensing on independent channels and complex wiring. This design provides a structural basis for balancing wide-area sensing, flexible conformability, and low-cost integration and supports the subsequent sensing-performance evaluation and interactive-application validation.

3. Sensing performance characterization of the bio-inspired hierarchical flexible fabric glove

Response speed, repeatability, and signal stability under practical working conditions are key metrics for evaluating flexible wearable tactile sensors [43–47]. To systematically characterize the tactile glove under different operating modes and loading conditions, the experiments first establish its basic performance boundaries through system-level dynamic response, node-level transient response, quasi-static pressure response, spatial consistency, repeated-loading stability, loading–unloading hysteresis, low-pressure detection, dynamic cyclic response, and long-term cyclic durability. The evaluation is then extended to the complete array and practical working conditions, focusing on spatial localization and signal interference under multipoint loading, dynamic adaptability at different excitation frequencies, and response variations caused by continuous wearing and finger bending.

First, the system-level dynamic response was measured while the glove operated in its normal full-matrix scanning mode. During the experiment, the system continuously read all tactile nodes, and a representative loading–release curve was extracted from the output sequence during rapid pressing, as shown in Fig. 3a. The apparent response and recovery times were approximately 90 ms and 80 ms, respectively, indicating that the glove can update local contact states on a hundred-millisecond timescale during normal full-matrix operation and provide timely tactile input for dynamic grasping, motion monitoring, and tactile interaction.

This response speed is on the same order of magnitude as that of representative tactile sensors [11,22,23,48] and is shorter than the reported behavioral reaction time to tactile stimulation in humans [49]. Because the result includes the effects of system scanning and manual loading, it primarily characterizes the dynamic update capability of the complete glove under practical operation and should not be interpreted as the intrinsic response speed of a single node. To further evaluate the response of a tactile node to high-speed transient loading, a ball-drop impact–release experiment was performed in a single-node high-speed acquisition mode. Only one node was enabled in this mode to reduce the time overhead of matrix scanning and channel switching. As shown in Fig. 3b, the apparent 10–90% rise time and 90–10% fall time were approximately 0.5 ms and 1.1 ms, respectively, indicating that the local sensing structure can capture millisecond-scale transient contact events.

The quasi-static pressure response of a representative node was then measured over 0–400 kPa. As shown in Fig. 3c, the output voltage increased continuously and monotonically with pressure in a nonlinear manner, and the repeated curves showed limited dispersion, indicating good repeatability and stability over a wide pressure range. This range covers both light contact and relatively strong pressing. Reported local peak pressures during activities of daily living can exceed 200 kPa and reach 268.3 kPa [50], suggesting that the measurement range of the glove covers most daily grasping and pressing tasks.

Stable behavior of a single node does not directly represent the consistency of the full-palm array. Therefore, five tactile nodes at representative glove locations were selected for quasi-static loading over the same 0–400 kPa range to compare their response amplitudes and trends. As shown in Fig. 3d, all five nodes exhibited consistent nonlinear pressure-response trends, although their baselines and amplitudes differed because of fabric stitching, local contact conditions of the piezoresistive material, and interlayer conformity. After zero-load baseline correction, the coefficients of variation of the five representative nodes were 7.63–15.02% over 30–380 kPa, indicating relatively consistent spatial responses at medium and high pressures. The coefficient of variation in the low-pressure region was approximately 32.38%, mainly because the small effective response amplitude amplified the relative influence of initial contact differences.

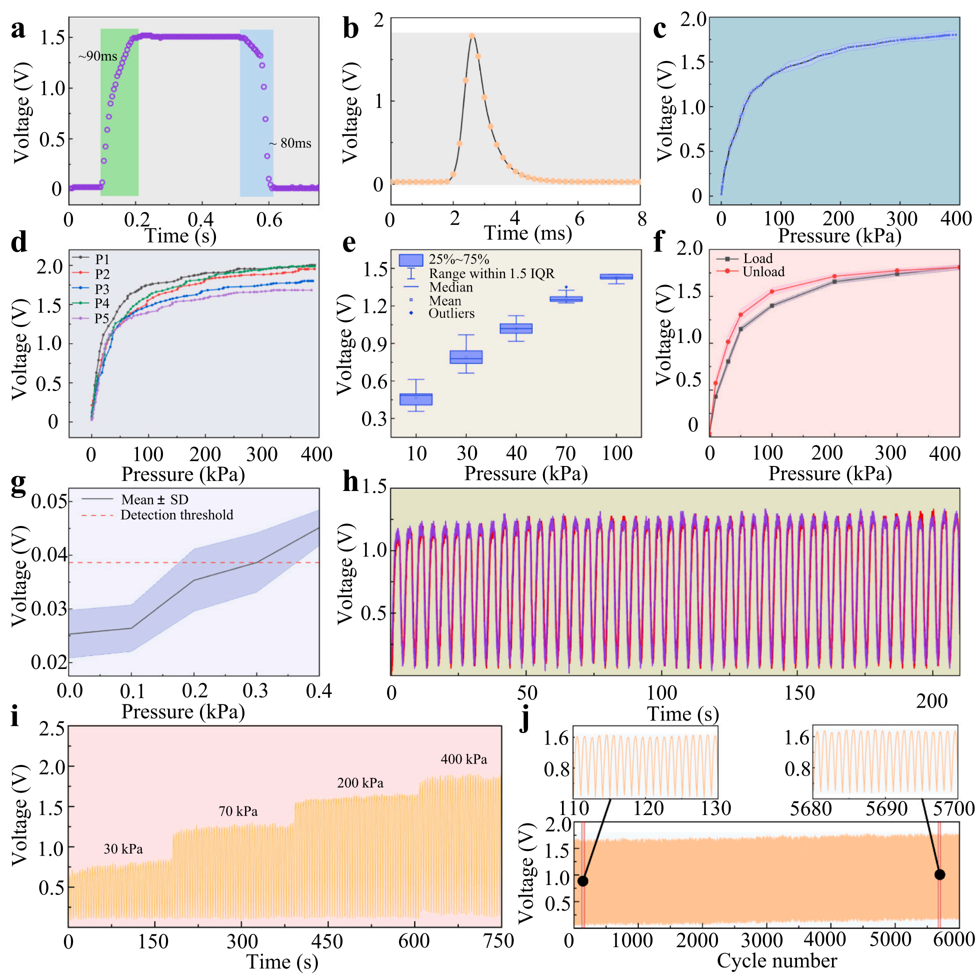

Fig. 3. Basic sensing performance and cyclic stability of the tactile glove under controlled loading. **a** System-level dynamic response of the complete glove under normal matrix-scanning operation; **b** local transient response of a single tactile node under high-speed impact–release; **c** pressure–voltage response and error range of the same node under quasi-static loading from 0 to 400 kPa; **d** comparison of the pressure responses of five representative nodes over 0–400 kPa; **e** response distributions over 20 repeated loadings at 10, 30, 40, 70, and 100 kPa; **f** hysteresis of a tactile node during a 0–400–0 kPa loading–unloading cycle; **g** low-pressure response and minimum detectable pressure; **h** comparison of two independent cyclic-loading experiments at 30 kPa; **i** dynamic responses under cyclic loading at 30, 70, 200, and 400 kPa; **j** durability over 6000 loading cycles.

Short-term repeatability was evaluated by applying 20 loading cycles at 10, 30, 40, 70, and 100 kPa. As shown in Fig. 3e, the response distributions at each pressure were concentrated, with small interquartile ranges and limited overall fluctuations. The median response increased regularly with pressure, and no obvious abnormal drift was observed. These results indicate that the tactile node maintains relatively stable output during short-term repeated contact.

In addition to repeatability along the same loading path, textile piezoresistive materials can exhibit path dependence during loading and unloading because of viscoelastic recovery, fiber friction, and conductive-network reconstruction. A quasi-static 0–400–0 kPa loading–unloading test was therefore performed, as shown in Fig. 3f. The unloading curve was generally higher than the loading curve at the same pressure, forming a discernible hysteresis loop. Based on the mean loading and unloading curves and full-scale normalization, the hysteresis error was 11.83% FS. Although the node exhibits a certain degree of hysteresis, the loading and unloading curves retain consistent response trends, supporting contact-event detection, pressure-level discrimination, and evaluation of dynamic grasp states.

The above measurements established the response characteristics at medium and high pressures. To determine the low-pressure detection boundary, repeated measurements were performed from 0 to 0.4 kPa, with 20 trials at each pressure, as shown in Fig. 3g. The detection threshold was defined as the mean zero-load output plus three standard deviations. Only 9 of 20 measurements at 0.3 kPa exceeded this threshold, whereas 19 of 20 measurements at 0.4 kPa did so. Accordingly, 0.4 kPa was identified as the experimentally verified minimum detectable pressure, demonstrating sub-kilopascal contact-detection capability.

After static and quasi-static characterization, the dynamic reproducibility of the node under continuous periodic loading was evaluated. A cyclic pressure of 30 kPa was applied to the same node in two independent experiments. As shown in Fig. 3h, the two response curves overlapped closely; the output rose rapidly during loading and returned near the baseline after unloading. The node therefore exhibited good dynamic reproducibility during short-term cyclic loading.

After confirming cyclic reproducibility at 30 kPa, the cyclic pressure was successively increased to 70, 200, and 400 kPa to evaluate discrimination among dynamic pressure amplitudes. As shown in Fig. 3i, the response amplitude increased stepwise with pressure, and clear, continuous periodic waveforms were retained at each pressure level without obvious peak attenuation or waveform instability. The piezoresistive textile node can therefore respond to both low-intensity repeated contact and higher-intensity periodic loading.

Finally, the cyclic evaluation was extended from short-term reproducibility to long-term durability. As shown in Fig. 3j, the effective response amplitudes before and after 6000 loading cycles were nearly identical, with a response-amplitude retention of 99.4% and an overall coefficient of variation of 2.8%. No obvious sustained degradation in device-level output was observed over the tested cycle range. A degree of zero-load baseline drift occurred during the test, but its influence can be reduced by zero-point calibration or baseline subtraction.

Fig. 3 establishes the basic performance boundaries of the tactile glove under controlled loading in terms of system- and node-level temporal responses, static electromechanical conversion, measurement consistency, dynamic reproducibility, and long-term cyclic durability. The complete matrix-scanning system and individual tactile nodes both show the basic capability to acquire tactile signals stably. However, the measurements in Fig. 3 are mainly based on controlled single-point loading and representative nodes and therefore do not fully characterize localization and operational stability of the complete array under multipoint contact, different loading frequencies, practical wearing, and finger deformation. The evaluation is consequently extended from single nodes and controlled loading to the complete array and practical working conditions, with emphasis on spatial signal quality, frequency adaptability, and robustness to wearing and deformation.

First, apparent node responses were evaluated under four conditions: loading without wearing, loading during wearing, bending without external load, and loading during bending, as shown in Fig. 4a. Practical wearing and finger bending increased the apparent responses of neighboring nodes, possibly because of the combined effects of hand soft-tissue deformation, expansion of the contact area, and load spreading through the textile. Although bending introduced baseline changes and neighboring-node responses, the dominant signal remained concentrated near the actual loaded region, and the loading location remained generally identifiable. Posture-dependent baseline correction may further reduce bending interference.

To distinguish mechanical load spreading during practical wearing from potential interference in matrix readout, a controlled simultaneous two-node loading experiment was first conducted, as shown in Fig. 4b. Two nodes located in different rows and columns were selected as the actual loading positions, with mean responses of 1.450 V and 1.402 V. Neither of the two unloaded cross-points formed by the corresponding row–column combinations exhibited an obvious response above the detection threshold. The maximum apparent adjacent-response ratios for the two loaded regions were 7.86% and 12.55%, and the maximum remote same-row/same-column response ratios were 2.21% and 2.85%, respectively. Under the representative conditions tested, non-target responses were concentrated primarily near the loaded nodes, and no obvious cross-point ghost response was observed.

Single-node loading experiments were subsequently conducted at three representative positions. The maximum apparent adjacent-response ratio was defined as the largest response among the eight neighboring nodes divided by the response of the target node, whereas the maximum remote same-row/same-column response ratio was defined as the largest response among remote nodes in the same row or column divided by the target-node response. Across the three loading positions, the maximum apparent adjacent-response ratios ranged from 9.52% to 12.82%, and the maximum remote same-row/same-column response ratios ranged from 1.00% to 4.97%. Because neighboring-node responses can be jointly affected by mechanical load spreading through the textile, loading-position deviation, and matrix-readout interference, they are described here as "apparent adjacent responses" rather than being attributed entirely to electrical crosstalk. These results indicate that the array retains identifiable dominant contact locations under the tested conditions.

After confirming spatial signal quality, the variation in node-output amplitude with pressure was quantified. Based on the nonlinear pressure–voltage curve in Fig. 3c, slopes over different pressure intervals were calculated using piecewise linear least-squares fitting, as shown in Fig. 4c. The corresponding sensitivities were 36.25, 6.330, 1.858, and 0.6118 mV/kPa over the pressure ranges of 0–30, 30–100, 100–200, and 200–400 kPa, respectively. The node exhibited higher sensitivity in the low-pressure range. As pressure increased, the output increment per unit pressure decreased and the segmented sensitivity declined, while the response remained monotonic throughout the test range. This analysis quantitatively complements the wide-range response in Fig. 3c and indicates that the node combines light-contact detection with a broad pressure range.

Fig. 3h and **i** mainly evaluate response reproducibility under specified cyclic conditions and discrimination among different pressure amplitudes, whereas **Fig. 4d** and **e** vary the excitation frequency to assess adaptability to loading-rate changes. At the same pressure amplitude, continuous and stable periodic outputs were obtained under both 5 Hz and 0.1 Hz cyclic loading. Relative to the quasi-static response at 0.1 Hz, the response-amplitude retention at 5 Hz was approximately 94.7%, with only slight attenuation. The node therefore covers dynamic processes ranging from slow pressing to rapid repeated contact.

After the spatial and frequency-domain evaluations under controlled loading, the combined influence of continuous wearing on sensing performance was examined. Six representative nodes were compared before and after the glove was worn continuously for 6 h, as shown in

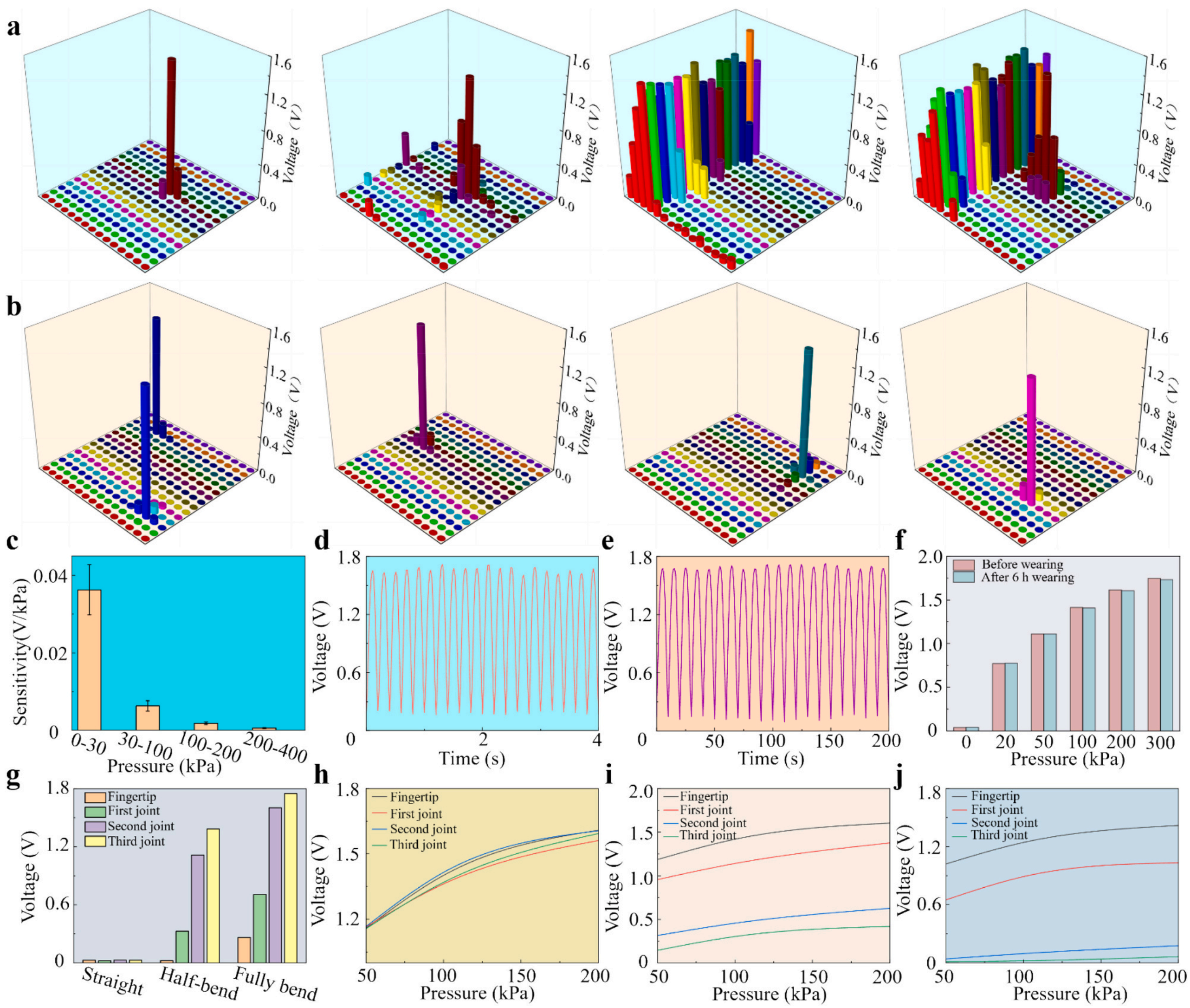

Fig. 4. Array-level signal quality and practical wearing adaptability of the tactile glove. a Spatial array responses and apparent inter-node responses under different wearing and finger-posture conditions, from left to right: single-point loading without wearing, single-point loading during wearing, zero-load response during wearing with the finger bent, and single-point loading during wearing with the finger bent; **b** ghost-signal distribution under simultaneous loading of two nodes and apparent adjacent-response distributions for three single-node loading positions; **c** segmented sensitivities over different pressure ranges; **d** dynamic response under 5 Hz high-frequency cyclic loading; **e** dynamic response under 0.1 Hz low-frequency cyclic loading; **f** pressure-response stability before and after 6 h of continuous wearing; **g** baseline interference induced by different bending states under zero load; **h** pressure–voltage responses at four representative locations with the finger straight; **i** pressure–voltage responses at four representative locations with the finger half-bent; **j** pressure–voltage responses at four representative locations with the finger fully bent.

Fig. 4f. Over 20–300 kPa, the mean response change at each pressure remained within approximately ±0.9%, while only a slight zero-load baseline change was observed. Under the ordinary indoor conditions of this continuous-wearing test, the combined effects of wearing for 6 h did not cause an obvious reduction in effective pressure response.

Finally, finger bending, the most direct structural deformation encountered during glove use, was evaluated in terms of baseline variation and compression of the pressure-response range. The experimental setup and three bending postures are shown in Supplementary Fig. S8, and the results are presented in Figs. 4g–4j. Under zero load, the baseline of nodes near the joints increased to different extents as the finger changed from straight to half-bent and fully bent because of fabric stretching, local folding, interlayer compression, and changes in the contact state. Under normal loading, the fingertip and first-joint regions retained relatively stable pressure responses, whereas the severely folded regions near the second and third joints showed more pronounced baseline drift and compression of the response range. Owing to this spatial difference, posture-dependent baseline calibration and region selection can be used to reduce residual bending interference. Nodes that retain an effective pressure response during bending can be corrected using their zero-load output at the corresponding posture, whereas nodes in severely folded regions with substantially compressed response ranges can be masked or down-weighted during pressure estimation or regional-feature calculation to reduce the risk of interpreting bending-induced apparent signals as external contact pressure.

In summary, this section first verifies the basic sensing performance of the tactile glove under controlled conditions in terms of dynamic response, pressure detection, repeatability, and durability, and then evaluates array operation under multipoint contact, different loading frequencies, continuous wearing, and finger bending. The glove retains identifiable full-palm tactile output together with good dynamic tracking and cyclic stability, although the low-pressure region exhibits relatively large node-to-node variation, the loading–unloading response shows hysteresis, and severely bent regions remain susceptible to deformation interference. Per-node calibration, zero-point correction, hysteresis compensation, and posture-dependent region selection can be used to further reduce the influence of node variation and structural deformation on quantitative pressure-measurement accuracy. These results provide an experimental basis for dexterous-hand teleoperation, shared tactile feedback, and exoskeleton-assistance triggering.

4. Interactive application validation of the bio-inspired hierarchical flexible fabric glove

The preceding experiments evaluated the tactile glove at two levels: basic sensing performance under controlled conditions and array adaptability under practical wearing conditions. The results characterized pressure response, spatial localization, dynamic tracking, cyclic stability, and bending interference. For tactile gloves intended for real human–machine interaction, however, stable pressure acquisition is only the foundation. The application experiments therefore examined whether the full-palm tactile matrix could be converted into task-specific inputs for downstream systems. Accordingly, application validation was conducted in three representative scenarios—five-finger dexterous-hand teleoperation, shared tactile feedback, and exoskeleton-assistance triggering—to evaluate the glove as a low-complexity and scalable tactile interaction interface.

Each frame from the full-palm tactile glove is a 15 × 15 tactile matrix covering the five fingers and palm. To construct a low-dimensional interface suitable for different downstream systems, the raw response of each node is first corrected using its zero-load baseline and normalized by its response gain, with the normalized value limited to 0–1. The 225 tactile nodes are then divided into six functional regions corresponding to the five fingers and palm, and the maximum normalized response in each region is extracted as the regional peak feature, forming a six-dimensional tactile feature vector. Compared with the regional

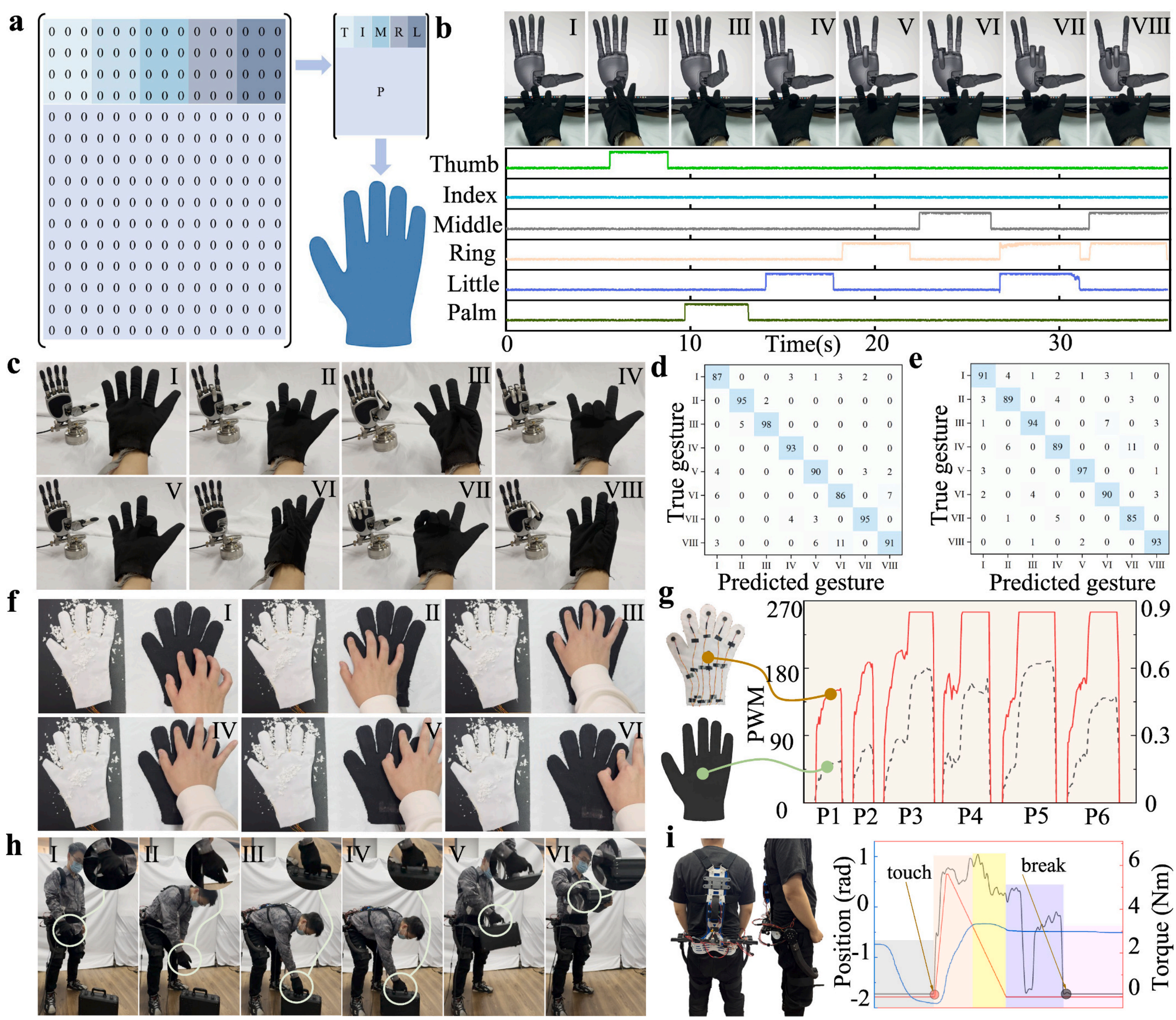

Fig. 5. Application validation of the full-palm tactile glove in representative interaction scenarios. a Mapping from the full-palm tactile matrix to a regional tactile feature vector; **b** tactile-glove-based teleoperation of a five-finger dexterous hand in MuJoCo and normalized tactile feature signals from the six functional regions; **c** physical five-finger dexterous-hand teleoperation; **d** confusion matrix of MuJoCo simulation teleoperation; **e** confusion matrix of physical dexterous-hand teleoperation; **f** shared tactile system composed of the tactile glove and a vibration-feedback glove; g tactile input and vibration-feedback responses in the shared tactile experiment; **h** tactile-glove-based triggering of hip-exoskeleton assistance during load handling; **i** tactile input and assistance output during the exoskeleton experiment.

mean, the peak feature better preserves the dominant responses produced by fingertip pressing, localized strong contact, and concentrated palm loading. This procedure compresses the 225-dimensional node response into six regional features at a compression ratio of 37.5:1. A first-order temporal filter is then applied to reduce frame-to-frame fluctuations, and the filtered features are used as control inputs for downstream systems (Supplementary **Table S2**). Meanwhile, the original 15 × 15 tactile matrix is retained for full-palm tactile-distribution reconstruction and visualization.

First, a five-finger dexterous-hand teleoperation experiment based on full-palm tactile information was constructed to determine whether the regional tactile features could be used for operator gesture recognition and robot-motion mapping. Conventional teleoperation generally relies on vision, inertial sensors, or dedicated hand-pose acquisition devices. In contrast, the present method uses the contact-pressure distribution generated between the fingers and glove during finger bending to extract regional features reflecting the bending state of each finger and uses these features as the control input for the dexterous hand.

During the experiment, the operator wore the tactile glove and performed multiple predefined gestures. The system acquired the full-palm tactile matrix in real time and extracted a six-dimensional tactile feature vector using regional peak features. This feature vector was then mapped to target joint commands for the five-finger dexterous hand, allowing the robotic hand to perform corresponding motions according to the operator's gesture. As shown in Fig. 5b, the method was first validated on the MuJoCo [51] physics-simulation platform. The virtual five-finger dexterous hand followed the input features to complete the corresponding gesture transitions and joint motions, indicating that regional tactile features can provide an effective input for dexterous-hand teleoperation.

Following the simulation validation, a physical five-finger dexterous-hand teleoperation experiment was conducted using a Linkerbot dexterous hand. As shown in Fig. 5c, the operator performed different predefined gestures while wearing the tactile glove, and the system converted the regional tactile features extracted in real time into control commands for the physical dexterous hand, driving the robotic hand to reproduce the corresponding postures.

The confusion matrices in **Fig. 5d** and **e** further show that the predefined gestures were distinguishable, supporting the usability of the regional tactile features for gesture recognition and motion mapping. These results indicate that the glove can serve not only as a full-palm tactile-data acquisition device, but also as a natural human–machine input interface for dexterous-hand teleoperation and tactile-driven robot control.

Second, to evaluate cross-end transmission of tactile information between the acquisition and feedback sides, a shared tactile system was constructed using a tactile acquisition glove and a vibration-feedback glove. In remote interaction, virtual reality, and collaborative operation, visual and auditory information can convey environmental states and action intentions but cannot directly represent contact position, force intensity, and their temporal variation. As shown in Fig. 5f, the acquisition side uses the full-palm tactile glove developed in this work to collect pressure distributions from the five fingers and palm in real time. The feedback side uses another glove integrated with six vibration motors to generate vibration at corresponding locations according to the tactile response of each functional region. Regional pressure information from the acquisition side is thus converted into perceptible position- and intensity-specific stimulation on the feedback side, forming a cross-end pathway from tactile acquisition to tactile feedback.

Fig. 5g further shows the temporal relationship between regional tactile features at the acquisition side and vibration output at the feedback side. The dashed lines represent the filtered normalized tactile features of the six functional regions, and the solid lines represent the PWM drive output of the corresponding vibration motors. To reduce false triggering caused by baseline fluctuations, the normalized trigger threshold was set to 0.03. When $F_i(t) < 0.03$, the corresponding vibration motor remained off, such that $\mathrm{PWM}_i(t) = 0$; when $F_i(t) \geq 0.03$, the regional feature was mapped to the vibration-driving intensity according to $\mathrm{PWM}_i(t) = \min\,[255, 195F_i(t) + 60]$. Thus, the contact region on the acquisition side determined the vibration location on the feedback side, whereas the tactile-response amplitude determined the drive intensity of the corresponding motor. The vibration feedback appeared, varied, and disappeared synchronously with the associated tactile signal. At a data-recording frequency of 25 Hz, the onset and offset of the two signals occurred within the same 40 ms sampling period, and no system-level signal-conversion delay longer than one sampling period was observed. These results verify position mapping, intensity conversion, and real-time transmission of tactile information between the acquisition and feedback sides.

Finally, the tactile glove was evaluated as a task-triggering interface for exoskeleton assistance. Common exoskeleton systems can trigger assistance through buttons, voice commands, preset timing, or posture sensors. During load handling, grasping, and collaborative operation, however, whether the hand has established effective contact with the target object is also an important indicator of task initiation. Detecting hand–object contact events with the tactile glove can therefore provide an assistance trigger directly related to the actual operation.

As shown in Fig. 5h, a hip-exoskeleton-assisted load-handling platform was constructed. The subject wore the full-palm tactile glove and the hip exoskeleton and grasped and carried a 5 kg box from the ground. When the subject bent down and contacted the box, the tactile array over the finger and palm regions detected the pressure change. The system interpreted the effective tactile response as the start signal of the handling task and triggered the hip exoskeleton to output assistive torque, supporting the transition from a bent posture to standing.

Fig. 5i shows the tactile input and assistance output during the exoskeleton experiment. The tactile trigger reflected the time at which the operator established contact with the target object, allowing exoskeleton output to correspond to the actual initiation of the handling task. This experiment verifies the feasibility of using a hand–object contact event as the task-triggering input for exoskeleton assistance and indicates that the tactile glove can serve as a task-sensing interface for wearable assistive devices in addition to robot teleoperation and shared tactile feedback.

In summary, application feasibility was validated in five-finger dexterous-hand teleoperation, shared tactile feedback, and exoskeleton-assisted load handling. Regional peak features extracted from the full-palm matrix characterized key hand-bending and contact states and were converted into robot control commands, vibration-feedback signals, or exoskeleton-assistance triggers. The glove can therefore function not only as a pressure-distribution acquisition device, but also as a lightweight, low-complexity, and scalable tactile interaction interface.

5. Conclusion

This work addresses the difficulty of balancing wide-area sensing, flexible conformability, and low-cost integration in existing tactile gloves by presenting a bio-inspired hierarchical flexible fabric glove for piezoresistive full-palm tactile sensing. Inspired by the hierarchical tactile sensing mechanism of human skin, the glove integrates a flexible fabric substrate, an orthogonal conductive-yarn network, carbon-containing piezoresistive fabric, and an insulating layer, enabling the glove body to provide structural support during wear, pressure transmission, electromechanical conversion, node addressing, and signal transmission. Using commercial textile materials, conventional sewing, and time-division-multiplexed matrix scanning, the glove forms a 15 × 15 tactile array containing 225 addressable nodes, while one glove together with its basic readout circuitry has a material cost of approximately US$5.

In terms of structure and readout, the glove uses a hierarchical sensing architecture composed of a near-palm longitudinal conductive layer, an insulating layer, a piezoresistive layer, and a far-palm transverse conductive layer. The near-palm and far-palm conductive layers form an orthogonal array and, together with the intermediate piezoresistive layer, define addressable tactile nodes. The insulating layer defines the effective sensing regions and reduces undesired conduction. Shift registers and a multiplexer sequentially select the row and column channels according to a predefined timing sequence, allowing the 225 nodes to be read through a limited number of connection leads and reducing the dependence of high-density tactile arrays on independent signal channels and complex wiring.

In terms of sensing performance, the system-level apparent response and recovery times under complete-matrix operation were approximately 90 ms and 80 ms, while the apparent rise and fall times in the single-node high-speed impact test were approximately 0.5 ms and 1.1 ms. The nodes exhibited a monotonic nonlinear pressure response over 0–400 kPa, an experimentally verified minimum detectable pressure of 0.4 kPa, and a loading–unloading hysteresis error of 11.83% FS. At medium and high pressures, the spatial coefficients of variation of five representative nodes were 7.63–15.02%. The response-amplitude retention was approximately 94.7% under 5 Hz dynamic loading and 99.4% after 6000 repeated loading cycles, indicating stable tactile output under the tested static, dynamic, and long-term cyclic conditions.

In terms of application validation, the 225-dimensional full-palm tactile matrix was compressed into six regional peak features and used for five-finger dexterous-hand teleoperation, shared tactile feedback, and hip-exoskeleton-assistance triggering. MuJoCo simulation and physical dexterous-hand experiments verified the feasibility of using regional tactile features for predefined-gesture recognition and motion mapping. The shared tactile experiment converted regional pressure information at the acquisition side into vibration location and intensity at the feedback side, while the exoskeleton experiment verified the feasibility of using hand–object contact events as triggers for load-handling assistance. These experiments primarily validate motion mapping, cross-end tactile feedback, and task-triggering functions; system-level applications in embodied-intelligence skill learning and high-precision remote operation require further investigation.

Overall, this study combines a bio-inspired hierarchical structure, textile-based fabrication, full-palm matrix sensing, and multi-scenario interaction input, achieving 225 addressable full-palm tactile nodes at a material cost of approximately US$5 for one glove and its basic readout circuitry. Compared with representative tactile sensing gloves, the proposed approach provides a relatively balanced combination of full-palm tactile coverage, structural integration, breathability, flexibility, and low cost (Supplementary **Table S3**). The work offers a low-cost route for wearable tactile systems to progress from local and add-on sensing toward full-palm coverage, fabric-level integration, and multi-task interaction.

The current system has several limitations. First, the piezoresistive array primarily responds to normal loads and cannot independently measure tangential forces during grasping and slipping or directly identify slip direction and friction state. Second, textile bending, stretching, local folding, and variations in interlayer contact cause fluctuations in node baselines and response gains. Posture-dependent baseline correction and region selection can reduce some of these effects but cannot completely eliminate coupling among different mechanical deformations. In addition, the current prototype relies mainly on manually assisted sewing; variations in stitch parameters and interlayer alignment can lead to differences in node response and batch consistency, limiting reproducibility in scaled manufacturing. Future work will improve sensing performance through multiaxial tactile sensing, mechanical-deformation decoupling, and fatigue-resistant structural design, and will enhance fabrication efficiency, manufacturing consistency, and scalability through programmable sewing, digital embroidery, standardized assembly, and automated node inspection.

CRediT authorship contribution statement

Yunsheng Ma: Writing – original draft, Visualization, Validation, Software, Methodology, Investigation, Formal analysis, Data curation, Conceptualization. **Xinran Li:** Methodology, Data curation. **Jiayi Wen:** Methodology, Conceptualization. **Jiaxin Huang:** Investigation. **Hanyu Liu:** Software. **Keqiang Ren:** Validation. **Tao Jian:** Visualization. **Zhihua Wang:** Visualization. **Zhigong Song:** Writing – review & editing, Supervision, Resources, Project administration, Funding acquisition, Conceptualization.

Declaration of competing interest

The authors declare that they have no known competing financial interests or personal relationships that could have appeared to influence the work reported in this paper.

Acknowledgements

This work was supported by the Wuxi Taihu Lake Talent Plan. This work was also supported by Linkerbot Beijing Technology Co., Ltd. The authors gratefully acknowledge the School of Mechanical Engineering, Jiangnan University for providing experimental facilities and support.

Appendix A. Supplementary data

Supplementary data to this article can be found online at https://doi.org/10.1016/j.cej.2026.181577.

Data availability

Data will be made available on request.

References

[1] B.P. Delhaye, F. Schiltz, F. Crevecoeur, et al., Fast grip force adaptation to friction relies on localized fingerpad strains, Sci. Adv. 10 (3) (2024) eadh9344.
[2] N. Zhang, J. Ren, Y. Dong, et al., Soft robotic hand with tactile palm-finger coordination, Nat. Commun. 16 (1) (2025) 2395.
[3] S. Suresh, H. Qi, T. Wu, et al., Neuralfeels with neural fields: visuotactile perception for in-hand manipulation, Sci. Robot. 9 (96) (2024) eadl0628.
[4] G. Xu, H. Wang, G. Zhao, et al., Self-powered electrotactile textile haptic glove for enhanced human-machine interface, Sci. Adv. 11 (12) (2025) eadt0318.
[5] M. Mohsan M, B. Hasanen B, T. Hassan, et al., A wearable thumb device for fruit firmness estimation with vision-based tactile sensing, Comput. Electron. Agric. 237 (2025) 110593.
[6] K.-H. Ha, J. Yoo, S. Li, et al., Full freedom-of-motion actuators as advanced haptic interfaces, Science 387 (6741) (2025) 1383–1390.
[7] J.J. Fleck, Z.A. Zook, J.P. Clark, et al., Wearable multi-sensory haptic devices, Nature Reviews Bioengineering 3 (4) (2025) 288–302.
[8] X. Wang, Z. Meng, C.Q. Chen, Enhancing haptic continuity in virtual reality using a continuity reinforcement skeleton, Nat. Commun. 16 (1) (2025) 2995.
[9] S.U. Park, H.K. Lee, H.B. Kim, et al., Wearable interactive full-body motion tracking and haptic feedback network systems with deep learning, Nat. Commun. 16 (1) (2025) 8604.
[10] H. Liu, Y. Shi, Y. Pan, et al., Sensory interactive fibers and textiles, NPJ Flexible Electron. 9 (1) (2025) 23.
[11] D. Lu, T. Liu, X. Meng, et al., Wearable triboelectric visual sensors for tactile perception, Adv. Mater. 35 (7) (2023) 2209117.
[12] C.C. Christoph, M. Eberlein, F. Katsimalis, et al., ORCA: an open-source, reliable, cost-effective, anthropomorphic robotic hand for uninterrupted dexterous task learning, arXiv preprint arXiv 250404259 (2025).
[13] H. Zhang, S. Hu, Z. Yuan, et al., DOGlove: dexterous manipulation with a low-cost open-source haptic force feedback glove, arXiv preprint arXiv:2502.07730, 2025.
[14] J. Zhao, N. Kuppuswamy, S. Feng, et al., PolyTouch: a robust multi-modal tactile sensor for contact-rich manipulation using tactile-diffusion policies, arXiv preprint arXiv:2504.19341, 2025.
[15] S. Chen, C. Wang, K. Nguyen, et al., Arcap: Collecting high-quality human demonstrations for robot learning with augmented reality feedback; proceedings of the 2025 IEEE International Conference on Robotics and Automation (ICRA), F, IEEE, 2025 [C].
[16] H. Lin, R. Corcodel, D. Zhao, Generalize by touching: Tactile ensemble skill transfer for robotic furniture assembly; proceedings of the 2024 IEEE International Conference on Robotics and Automation (ICRA), F, IEEE, 2024 [C].

[17] H. Jin, Y. Kim, W. Youm, et al., Highly pixelated, untethered tactile interfaces for an ultra-flexible on-skin telehaptic system, NPJ Flexible Electron. 6 (1) (2022) 82.
[18] S.Y. Kwon, G. Park, H. Jin, et al., On-skin and tele-haptic application of mechanically decoupled taxel array on dynamically moving and soft surfaces, NPJ Flexible Electron. 6 (1) (2022) 98.
[19] Z. Zhao, W. Li, Y. Li, et al., Embedding high-resolution touch across robotic hands enables adaptive human-like grasping, Nature Machine Intelligence 7 (6) (2025) 889–900.
[20] C. Jiang, W. Xu, Y. Li, et al., Capturing forceful interaction with deformable objects using a deep learning-powered stretchable tactile array, Nat. Commun. 15 (1) (2024) 9513.
[21] Q. Mao, Z. Liao, J. Yuan, et al., Multimodal tactile sensing fused with vision for dexterous robotic housekeeping, Nat. Commun. 15 (1) (2024) 6871.
[22] Y. Chen, J. Cao, J. Qiu, et al., Capacitive in-sensor tactile computing, Nat. Commun. 16 (1) (2025) 5691.
[23] Y. Liu, J. Wang, T. Liu, et al., Triboelectric tactile sensor for pressure and temperature sensing in high-temperature applications, Nat. Commun. 16 (1) (2025) 383.
[24] O. Ozioko, R. Dahiya, Smart tactile gloves for haptic interaction, communication, and rehabilitation, Adv. Intell. Syst. 4 (2) (2022) 2100091.
[25] J. Huang, K. Chen, J. Zhou, et al., Dih-tele: dexterous in-hand teleoperation framework for learning multiobjects manipulation with tactile sensing, IEEE/ASME Trans. Mechatron. 30 (5) (2025) 3840–3851.
[26] M. Burgess, E.H. Adelson, Grasp EveryThing (GET): 1-DoF, 3-fingered gripper with tactile sensing for robust grasping, arXiv preprint arXiv:2505.09771, 2025.
[27] J. Yin, H. Qi, Y. Wi, et al., OSMO: open-source tactile glove for human-to-robot skill transfer, arXiv preprint arXiv:2512.08920, 2025.
[28] P. Ruppel, J. Zhang, Elastic tactile sensor glove for dexterous teaching by demonstration, Sensors (Basel, Switzerland) 24 (6) (2024) 1912.
[29] S. Sundaram, P. Kellnhofer, Y. Li, et al., Learning the signatures of the human grasp using a scalable tactile glove, Nature 569 (7758) (2019) 698–702.
[30] Y.R. Song, J. Li, R. Fu, et al., OPENTOUCH: bringing full-hand touch to real-world interaction, arXiv preprint arXiv:2512.16842, 2025.
[31] Y. Luo, C. Liu, Y.J. Lee, et al., Adaptive tactile interaction transfer via digitally embroidered smart gloves, Nat. Commun. 15 (1) (2024) 868.
[32] T. Someya, T. Sekitani, S. IBA, et al., A large-area, flexible pressure sensor matrix with organic field-effect transistors for artificial skin applications, Proc. Natl. Acad. Sci. 101 (27) (2004) 9966–9970.
[33] B. Huang, Y. Wang, X. Yang, et al., 3D-VitaC: learning fine-grained manipulation with visuo-tactile sensing, arXiv preprint arXiv:2410.24091, 2024.
[34] G. Sun, Z. Sun, L. Liu, et al., Transparent conductive hydrogels with water-responsive contractility, repairability, and biocompatibility for visible conformal shape-adaptive tissue-adherent monitoring, Adv. Funct. Mater. 36 (22) (2026) e22718.
[35] S. Wang, X. Fan, Z. Zhang, et al., A skin-inspired high-performance tactile sensor for accurate recognition of object softness, ACS Nano 18 (26) (2024) 17175–17184.
[36] Z. Liu, X. Hu, R. Bo, et al., A three-dimensionally architected electronic skin mimicking human mechanosensation, Science 384 (6699) (2024) 987–994.
[37] H. Hu, C. Zhang, X. Lai, et al., Large-area magnetic skin for multi-point and multi-scale tactile sensing with super-resolution, NPJ Flexible Electron. 8 (1) (2024) 42.
[38] Q. Hua, J. Sun, H. Liu, et al., Skin-inspired highly stretchable and conformable matrix networks for multifunctional sensing, Nat. Commun. 9 (1) (2018) 244.
[39] Z. Yang, Y. Pang, X.-L. Han, et al., Graphene textile strain sensor with negative resistance variation for human motion detection, ACS Nano 12 (9) (2018) 9134–9141.
[40] R. Cao, X. Pu, X. Du, et al., Screen-printed washable electronic textiles as self-powered touch/gesture tribo-sensors for intelligent human–machine interaction, ACS Nano 12 (6) (2018) 5190–5196.
[41] G. Li, S. Liu, L. Wang, et al., Skin-inspired quadruple tactile sensors integrated on a robot hand enable object recognition, Sci. Robot. 5 (49) (2020) eabc8134.
[42] W.-M. Zhong, Q.-X. Liu, Y.-P. Jiang, et al., Ultra-high dielectric tuning performance and double-set resistive switching effect achieved on the Bi2NiMnO6 thin film prepared by sol–gel method, J. Colloid Interface Sci. 606 (2022) 913–919.
[43] G. Sun, D. Wang, P. Wang, et al., A flexible temperature sensor with ultrafast response speed and high stability achieved by improving substrate thermal conductivity and radiative cooling, Adv. Funct. Mater. 36 (2) (2026) e12296.
[44] G. Sun, Z. Ma, Z. Xiao, et al., All-fiber-type temperature sensor powered by zinc-ion battery toward wearable sensing clothes for health monitoring, Adv. Funct. Mater. 36 (20) (2026) e18490.
[45] S.-M. Li, X.-G. Tang, Y.-C. Chen, et al., Emerging triboelectric nanogenerator-based neuromorphic electronics: from self-powered sensing to bioinspired synapses, Results Eng. 30 (2026) 111295.
[46] J.-C. Fan, X.-G. Tang, Q.-J. Sun, et al., Low-cost composite film triboelectric nanogenerators for a self-powered touch sensor, Nanoscale 15 (13) (2023) 6263–6272.
[47] Q.-Z. Ren, L.-H. Nie, D.-L. Li, et al., Flexible memristors based on ZrO2/ZnO heterojunctions for neuromorphic computing, Mater. Sci. Semicond. Process. 206 (2026) 110445.
[48] Y. Qiu, Z. Wang, P. Zhu, et al., A multisensory-feedback tactile glove with dense coverage of sensing arrays for object recognition, Chem. Eng. J. 455 (2023) 140890.
[49] D.J. Caldwell, J.A. Cronin, J. Wu, et al., Direct stimulation of somatosensory cortex results in slower reaction times compared to peripheral touch in humans, Sci. Rep. 9 (1) (2019) 3292.
[50] J. Cepriá-Bernal, A. Pérez-González, Dataset of tactile signatures of the human right hand in twenty-one activities of daily living using a high spatial resolution pressure sensor, Sensors (Basel, Switzerland) 21 (8) (2021) 2594.
[51] E. Todorov, T. Erez, Y. Tassa, Mujoco: A physics engine for model-based control; proceedings of the 2012 IEEE/RSJ International Conference on Intelligent Robots and Systems, F, IEEE, 2012 [C].